© 1989 Birkhäuser Verlag, Basel

Full-Correlation Analysis of Turbulent Scattering Layers in the Mesosphere Observed by the MU Radar

MAMORU YAMAMOTO,[1] TORU SATO,[1] TOSHITAKA TSUDA,[1] SHOICHIRO FUKAO[1] and SUSUMU KATO[1]

Abstract—We have applied a full-correlation analysis technique to the echo power fluctuations observed by the MU radar (35°N, 136°E), and analyzed the horizontal structure of the scattering pattern in the mesosphere as well as their horizontal motions. The velocity of the scattering pattern did not agree with the background wind velocity, but was associated with the horizontal propagating direction of a saturated inertia gravity wave identified in the wind field. The length of the long axis of the characteristic ellipse of the scattering pattern was approximately 50 km, and the direction was almost perpendicular to the propagating direction of the wave. The correlation time of the scattering pattern was approximately 700 s, which is much longer than the lifetime of the isolated turbulence itself. This implies that the observed scattering pattern is associated with a region where the saturated inertia gravity wave generates turbulence.

Key words: MU radar, mesosphere, turbulence, scattering layer, full-correlation analysis technique, gravity wave, wave breaking.

1. Introduction

Theoretical works have revealed that the gravity wave breaking in the mesosphere produces instabilities, and the mean wind is accelerated by the momentum deposition of the gravity wave (LINDZEN, 1981; HOLTON 1982). The acceleration of the mean wind has been observed using a partial reflection radar by calculating the convergence of the momentum flux due to the gravity waves (VINCENT and REID, 1983; FRITTS and VINCENT, 1987). On the other hand, MST radars detect returns from turbulence which is expected to be generated by dissipating gravity waves in the mesosphere. Echo power observed by the MST radars is a good measure of intensity of turbulence, and can be utilized to obtain refractivity turbulence structure constant C_n^2 in the atmosphere (VANZANDT *et al.*, 1978). Evidence of the relationship between turbulence layers and gravity waves was shown by YAMAMOTO *et al.* (1988), where they observed that turbulence scattering layers in the mesosphere appear around the altitudes where gravity waves are most unstable.

[1] Radio Atmospheric Science Center, Kyoto University, Uji, Kyoto 611, Japan.

Horizontal motions of echo power bursts in the mesosphere were observed by KLOSTERMEYER and RÜSTER (1984) and RÜSTER and KLOSTERMEYER (1987) by calculating the cross-correlation functions between echo power bursts observed in beams pointing in the different directions, although they did not consider the random changes of the scattering pattern in time. RÜSTER and KLOSTERMEYER (1987) have shown that motions of the echo power bursts agree with the background wind on average. Full-correlation analysis is a technique to observe the structure and motion of horizontal patterns by taking the spatial correlation into account (BRIGGS, 1984). This technique is utilized with both MF partial reflection and VHF radar observations in order to obtain horizontal wind velocities from the fading patterns detected by three spatially separated receivers.

The MU radar (35°N, 136°E), which has been operated since 1983, is a monostatic pulse Doppler radar with a carrier frequency of 46.5 MHz (KATO *et al.*, 1984; FUKAO *et al.*, 1985a,b). The advantage of the MU radar over conventional MST radars is that the MU radar can steer its beam every Inter-Pulse-Period so that it can observe several areas which are spatially separated from each other almost simultaneously. This capability enables us to investigate small-scale structure in the turbulence and wind fields.

A saturated gravity wave has been found by YAMAMOTO *et al.* (1987) in the mesosphere by the MU radar observations on February 8, 1985. The gravity wave produced a region with negative Richardson number and with large fluctuations in radial wind velocities, which implied that the wave dissipated its energy through shear or convective instabilities. In this paper, we apply the full-correlation analysis to this saturated gravity wave in order to observe horizontal structures of the scattering layers, and investigate the generation of turbulence by the saturated gravity wave.

2. Full-correlation Analysis

Observations of the mesosphere were carried out on February 8, 1985 using the parameters shown in Table 1. Using a least squares fitting method, we determined echo power, radial wind velocity and spectral width from the power spectrum of radar returns. The height and time resolution of the observations were 300 m and two minutes, respectively. As shown in Figure 1, we used four beams, pointing northward, eastward, southward and westward with a zenith angle of 10°. Thus we could observe the echo power at four spatially separated positions.

Figure 1 schematically shows the horizontal pattern of the echo power that moves with velocity V. We assume that the pattern $f(x, y, t)$ of echo power is a function of position (x, y) and time t, where x and y-axes correspond to the

Table 1

Observation parameters of the MU radar.

Observation period	February 8, 1985
Observation range	60–98.1 km
Number of beams	4
Beam direction	Northward ($\theta = 10°$)
(θ: Zenith angle)	Eastward ($\theta = 10°$)
	Southward ($\theta = 10°$)
	Westward ($\theta = 10°$)
Range resolution	300 m
Time resolution	120 s
Inter pulse period	730 μs
Pulse compression	16 bit complementary
Coherent integration	30 times
Incoherent integration	10 times

eastward and northward directions, respectively. The spatial and time scales of the horizontal pattern is described by the three dimensional correlation function

$$\rho(\xi, \eta, \tau) = \frac{\langle f(x, y, t) f(x + \xi, y + \eta, t + \tau) \rangle}{\langle \{f(x, y, t)\}^2 \rangle}, \tag{1}$$

where $\langle\rangle$ denotes an average, τ is the time lag and ξ and η are spatial lags along the x and y-axes, respectively. The correlation function can be approximated by a family of concentric ellipsoids with the center at the origin (BRIGGS, 1984). We therefore write

$$\rho(\xi, \eta, \tau) = \rho(A\xi^2 + B\eta^2 + C\tau^2 + 2F\xi\eta + 2G\eta\tau + 2H\xi\eta), \tag{2}$$

where A, B, C, F, G and H are constants. Here, we assume that the correlation function is described by an exponential function as follows

$$\rho(\xi, \eta, \tau) = \exp\{-(A\xi^2 + B\eta^2 + C\tau^2 + 2F\xi\eta + 2G\eta\tau + 2H\xi\eta)\}. \tag{3}$$

Because we observe echo power in the four beams, the cross-correlation functions between echo power observed in different beams can be described by $\rho(\xi, \eta, \tau)$; *e.g.*, the cross-correlation function between the echo power observed in the northward beam $(0, \eta_0)$ and the eastward beam $(\xi_0, 0)$ corresponds to $\rho(\xi_0, -\eta_0, \tau)$. In order to determine the parameters of Eq. (3), we have utilized a least squares fitting technique to the cross-correlation function between the echo power in the four beams. An example of the cross-correlation functions is shown in Figure 2, which corresponds to the scattering pattern observed in 10–16 LT at 71.4 km. In this figure, we chose three cross-correlation functions of the echo power observed in the beams pointing eastward, southward and westward, although we used the

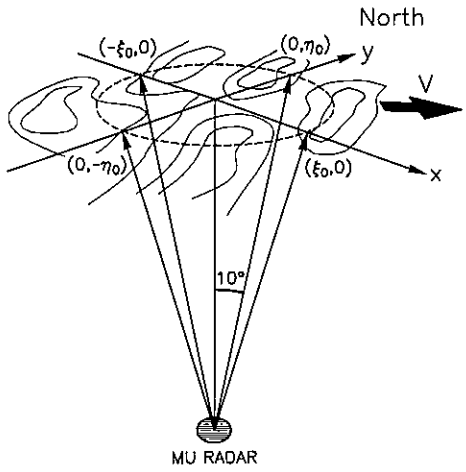

Figure 1
Beam assignment used in the MU radar observations on February 8, 1985 together with a schematic diagram of the scattering pattern which moves horizontally with velocity V, where x and y-axes correspond to the eastward and northward directions, respectively.

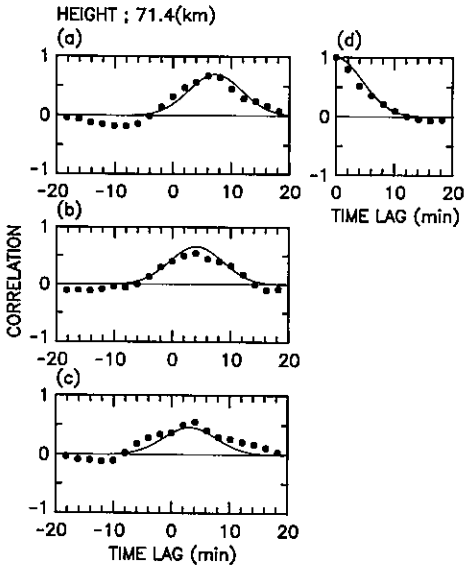

Figure 2
Cross-correlation functions between echo power observed in 10–16 LT at 71.4 km. The panels (a), (b) and (c) correspond to the cross-correlation functions obtained between the southward and eastward, the southward and westward and the westward and eastward beams, respectively. The echo power in the eastward beam lags behind that in the southward beam, the westward behind the southward, and the eastward behind the westward. The panel (d) shows the autocorrelation function averaged over all beams. The solid line in each panel corresponds to $\rho(\xi, \eta, \tau)$ obtained by using the least squares fitting method.

cross-correlation functions with all the combinations of the four beams in the determination of the parameters. The auto-correlation function used is an average of those calculated in the four beams. The solid curves in Figure 2 show the result of the fitting. We cannot apply the fit to the negative correlation coefficients because of Eq. (3), but the fitted curves are close to the observed values for positive correlation coefficients.

When we obtain the parameters, the horizontal velocity of the scattering echo pattern is calculated as a 'tilt' of one axis of the ellipsoids relative to the τ-axis. The x and y components of V are V_x and V_y, respectively, and are given by

$$AV_x + HV_y = -F$$
$$HV_x + BV_y = -G \tag{4}$$

(BRIGGS, 1984). The motion of the scattering pattern shown in Figure 2 has been estimated to be $V_x = 9.6\ \mathrm{ms}^{-1}$ and $V_y = 27.5\ \mathrm{ms}^{-1}$. In order to find a spatial scale for the scattering pattern, the particular ellipse for which $\rho = 0.5$ may be defined as the 'characteristic ellipse', which is described by

$$A\xi^2 + B\eta^2 + 2H\xi\eta = C\tau_{0.5}^2, \tag{5}$$

where $\tau_{0.5}$ is a time lag at which the autocorrelation function is equal to 0.5, *i.e.*, $\rho(0, 0, \tau_{0.5}) = 0.5$ (BRIGGS, 1984).

3. Results

Figure 3 shows a time-height distribution of the scattering layer observed on February 8, 1985 (after YAMAMOTO *et al.*, 1987). Within the scattering layers, we find an intense and thick scattering region during 12–16 LT at 69–73 km, which

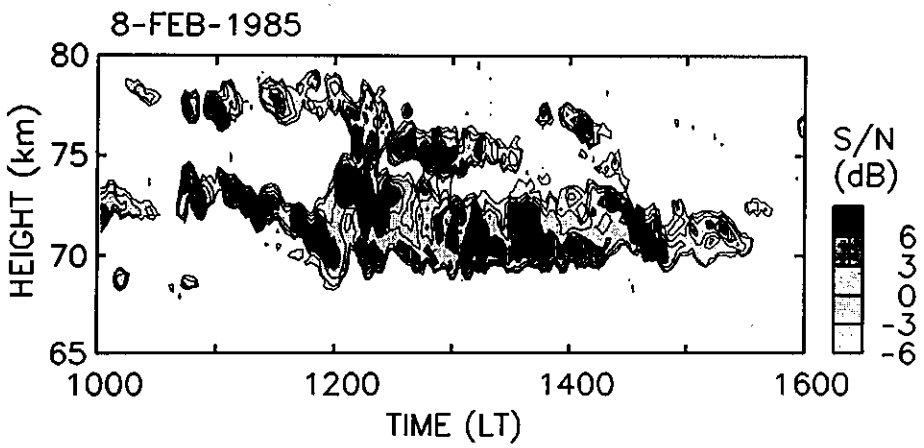

Figure 3
Time-height sections of the signal-to-noise ratio observed in the southward beam on February 8, 1985 (after YAMAMOTO *et al.*, 1987).

consists of many isolated patchy structures. We have tried the full-correlation analysis for the data observed during 10–16 LT at 69–73 km, and the fitting was successful at 69.4–71.7 km. Figure 4 shows the motion of the scattering pattern. All of the data are distributed in the region with positive V_x and V_y, and show that the fluctuation patterns in this altitude range move toward the north-northeast. The average of the horizontal velocities, which is shown by an arrow, is $V_x = 9.5\ \mathrm{ms}^{-1}$ and $V_y = 24.2\ \mathrm{ms}^{-1}$.

The characteristic ellipses of the scattering pattern are shown in Figure 5. The size and the direction of these ellipses are similar to each other. The long axes of the ellipses lie in the east-west direction, which is almost perpendicular to V. The length of the long and short axes of the characteristic ellipse, which show the spatial scale of the scattering pattern, are approximately 50 and 20 km, respectively. Because the three-dimensional correlation function for the scattering patterns is obtained, we can calculate the correlation time along the horizontal motion of the pattern. As shown in Figure 6, they are approximately 700 s at all altitudes.

As shown by YAMAMOTO *et al.* (1987), we could recognize a clear monochromatic wave-like structure in the wind profile. The vertical wavelength was approximately 5.6 km. Figure 7 shows a hodograph of the wind vector in 1230–1330 LT at 68.8–76.5 km (after YAMAMOTO *et al.*, 1987), which is obtained after subtracting the vertical linear trend of the profile. The tip of the wind vector moves clockwise with increasing height throughout the whole altitude range. The elliptic motion of the wind vector implies that the wave is an inertia gravity wave, and its energy propagates upward. The intrinsic period of the wave is estimated to be 8 hr from the ratio between long and short axes of the elliptic motion in the hodograph. YAMAMOTO *et al.* (1987) has inferred that the inertia gravity wave propagates

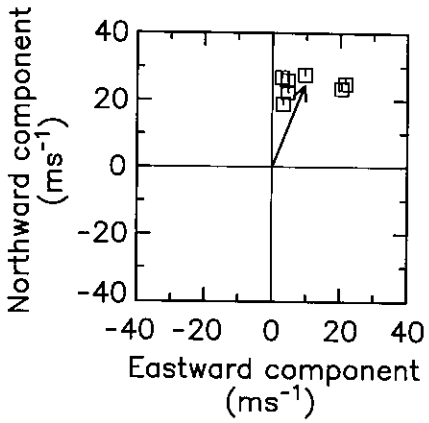

Figure 4
Horizontal motion of the scattering pattern observed in 10–16 LT in the altitude region of 69–72 km. A square symbol denotes the tip of the velocity vector obtained by using the full-correlation method at each altitude. An arrow shows the averaged velocity vector.

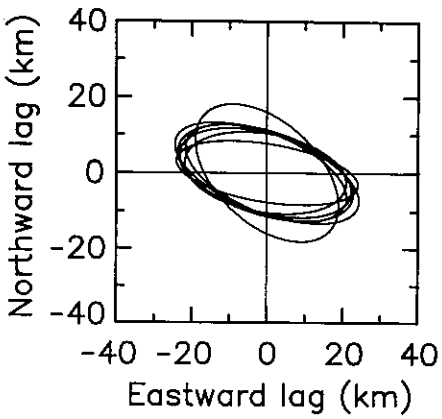

Figure 5
The characteristic ellipse of the scattering pattern observed in 10–16 LT in the altitude region of 69–72 km.

horizontally toward the north along the long axis of the ellipse. The horizontal wavelength of the gravity wave is approximately 600 km, and the horizontal phase velocity of the wave is 20 ms^{-1} toward the north. Also, they have calculated the Richardson number modified by the gravity wave, and found that the minimum Richardson number was slightly negative. This means that the gravity wave was saturated and the wave breaking set in.

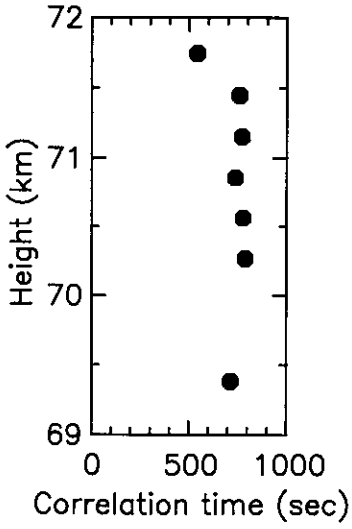

Figure 6
The correlation time of the scattering pattern along the horizontal motion observed in 10–16 LT in the altitude region of 69–72 km.

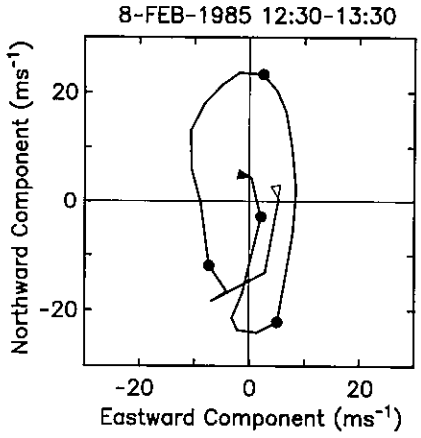

Figure 7
A polar plot of the wind velocity averaged over 1230–1330 LT on February 8, 1985. The vertical linear trend of the wind velocity is subtracted. The open and solid triangles indicate the lowest (68.8 km) and highest altitudes (76.5 km), respectively. Circular symbols are plotted at 70, 72, 74 and 76 km (after YAMAMOTO *et al.*, 1987).

Figure 8 shows a velocity profile averaged over 10–16 LT. The wind velocities still consist of the gravity wave component. We have calculated the vertical trend of the wind profile, which is more representative of the background wind than the wind profile itself. The zonal component of the vertical trend shows eastward velocity at all height range. The meridional component, on the other hand, changes

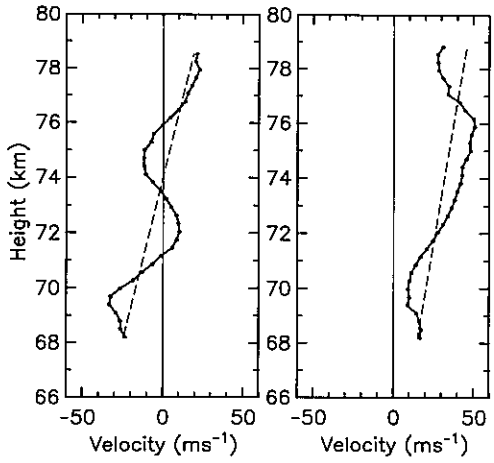

Figure 8
The wind profile averaged over 10–16 LT on February 8, 1985. Left and right panels correspond to the northward and eastward components, respectively. Dashed lines show the vertical linear trend of the wind profile.

its sign around 74 km. At the altitude of 70 km, the eastward and northward components of the vertical linear trend are 20 and $-17\ \mathrm{ms}^{-1}$, respectively, which means the background wind toward the southeast. This direction is not consistent with (V_x, V_y) shown in Figure 4. The horizontal phase velocity of the gravity wave is $20\ \mathrm{ms}^{-1}$ northward, which is similar to the averaged $V_y = 24.2\ \mathrm{ms}^{-1}$. The direction of the motion of the scattering pattern is better associated with the horizontal propagation direction of the gravity wave than of the background wind velocity.

4. Discussions

The contribution of the atmospheric turbulence to the spectral width σ measured by a radar is given by the integration of the three-dimensional kinetic energy spectrum of turbulence from k_0 to k_i, where k_0 is the wavenumber associated with the largest vortex in the turbulence, and k_i is the radar Bragg wavenumber, respectively (SATO and WOODMAN, 1982). If k_i is within the inertial subrange, it is given by

$$\frac{3}{2}\sigma^2 = \int_{k_0}^{k_i} \alpha \varepsilon^{2/3} k^{-5/3}\, dk, \tag{6}$$

where α is the Kolmogoroff's constant of about 1.6, and ε is the energy dissipation rate per unit mass and time. The MU radar observes turbulence with the 3-m scale, which is slightly less than the minimum scale of turbulence in the inertial subrange (*e.g.*, GAGE and BALSLEY, 1980). In this case, the integral in this equation must be modified to include the viscous dumping of the spectra. However, since $k_i \gg k_0$, this modification does not affect the result of the integration, so that ε can be written as

$$\varepsilon = \alpha^{-3/2} \sigma^3 k_0. \tag{7}$$

k_0 can be approximated as $k_0 = \omega_B/\sigma$, where ω_B is the Brunt-Väisälä frequency (WEINSTOCK, 1981). Assuming the turbulence energy per unit mass $E \sim \sigma^2$ and $\omega_B \approx 2 \times 10^{-2}$ s, the lifetime of the dissipating turbulence is estimated as

$$\tau_t = \frac{E}{\varepsilon} \approx \frac{2}{\omega_B} \sim 100(s). \tag{8}$$

This value is much smaller than the time scale of the scattering pattern shown in Figure 6.

As shown by FRITTS and RASTOGI (1985), the Brunt-Väisälä frequency is modified by the gravity wave, and ω_B becomes zero when the wave breaking sets in. In our analysis, the Richardson number modified by the gravity wave is possibly smaller than the background value at 69–72 km (YAMAMOTO *et al.*, 1987). The

lifetime of the dissipating turbulence can also be estimated by the thickness of the scattering layers. From Eq. (8) we can write

$$\tau_t = \frac{\sigma^2}{\alpha^{-3/2}\sigma^3 k_0} = \alpha^{3/2}\frac{L_0}{2\pi\sigma}, \tag{9}$$

where $L_0 = 2\pi/k_0$ is the diameter of the largest vortex in the turbulence layer. We assume $\sigma = 3$ m, which is consistent with the spectral width shown by YAMAMOTO *et al.* (1987). In order to estimate L_0, we refer to the thickness of the scattering layers. In the time-height distribution of the echo power (Figure 3), thickness of the contour region with the signal-to-noise ratio above 6 dB is typically 1 km and less than 2 km at 69–73 km. Assuming $L_0 = 1$ km, we obtain $\tau_t = 110$ s from Eq. (9). This value is consistent with that estimated by using Eq. (8), and is less than the observed time scale.

RÖTTGER and IERKIC (1985) have observed horizontal trajectories of turbulence blobs in the mesosphere. The motions were detected by using the interferometer technique within 3–4 km of the echoing region of the vertical beam. The blobs showed the horizontal motions in the same direction of the background wind determined by the Doppler shift. It is because the analysis technique is equivalent to the spaced antenna drift and Doppler shift measurements. The interferometer technique traced the motion of the isolated region of turbulence itself. In our analysis, on the other hand, the distance between echoing regions of eastward and northward beams was approximately 17 km at the altitude of 70 km. Considering the large correlation time of the scattering pattern, the motion we observed is not the one of isolated turbulence detectable within a transmitting beam, but the motion of the region where turbulence is being generated. Another filtering effect may arise because we used the echo power averaged in the echoing region, while RÖTTGER and IERKIC (1985) could detect the micro-structures inside the beam.

KLOSTERMEYER and RÜSTER (1984) have observed the horizontal motion of the echo power bursts by using a simple correlation technique, and mentioned that the motion was identical to the background wind velocity. Because of their actual zenith angle of 6°, the distance between vertical and eastward beams was 8.4 km at the altitude of 80 km. It is not sure if the motion of the isolated turbulence was detectable with the grid of this size. It is possible that the trace velocities represented the same motion as that of our analysis. In our case, however, we observed the inertia gravity wave with the slightly negative Richardson number in the wind field, and the wave strongly produced turbulence through instabilities. Although KLOSTERMEYER and RÜSTER (1984) used the simple correlation technique, the differences in the analysis techniques do not largely affect the observational results since we still have the northward motion of the scattering pattern with the simple correlation technique.

Recently, RÜSTER and KLOSTERMEYER (1987) have statistically shown that the motion of the echo power bursts agrees with the background wind on average. The

horizontal spacing of the beams was 5 km at the altitude of 70 km, and the simple correlation technique was used. The motion of the echo power bursts distributed widely around the average, and the direction of the motion is sometimes different from that of the background wind by approximately 90°. The results of our analysis may be attributed to one of the extreme cases. We infer that the magnitude of gravity waves in the background wind field could change the situation whether the motion of the scattering pattern is parallel to the background wind or not.

5. Concluding Remarks

In this paper, we have shown a new technique to observe the horizontal motion of the scattering layers by fully utilizing the fast beam steerability of the MU radar. The full-correlation analysis technique has also allowed us to obtain the horizontal scale and the correlation time of the moving scattering pattern. The direction of the horizontal motion did not agree with that of the background wind velocity, but was associated with the horizontal propagation direction of the inertia gravity wave observed in the wind field. Because the gravity wave showed a negative Richardson number, we infer that the motion of the scattering pattern is that of the region where turbulence is locally generated by the saturated gravity wave.

Acknowledgement

The authors thank Drs. W. K. Hocking, J. Röttger and B. H. Briggs for helpful discussions and suggestions. The authors are also grateful to Dr. P. T. May for his careful reading of the manuscript. The MU radar belongs to, and is operated by the Radio Atmospheric Science Center, Kyoto University.

REFERENCES

BRIGGS, B. H. (1984), *The analysis of spaced sensor records by correlation techniques*, Handbook for MAP *13*, 166–186.

FRITTS, D. C., and RASTOGI, P. K. (1985), *Convective and dynamical instabilities due to gravity wave motions in the lower and middle atmosphere: Theory and observations*, Radio Sci. *20*, 1247–1277.

FRITTS, D. C., and VINCENT, R. A. (1987), *Mesospheric momentum flux studies at Adelaide, Australia: Observations and a gravity wave-tidal interaction model*, J. Atmos. Sci. *44*, 605–619.

FUKAO, S., SATO, T., TSUDA, T., KATO, S., WAKASUGI, K., and MAKIHIRA, T. (1985a), *The MU radar with an active phased array system, 1. Antenna and power amplifiers*, Radio Sci. *20*, 1155–1168.

FUKAO, S., TSUDA, T., SATO, T., KATO, S., WAKASUGI, K., and MAKIHIRA, T. (1985b), *The MU radar with an active phased array system, 2. In-house equipment*, Radio Sci. *20*, 1169–1176.

GAGE, K. S., and BALSLEY, B. B. (1980), *On the scattering and reflection mechanisms contributing to clear air radar echoes from the troposphere, stratosphere, and mesosphere*, Radio Sci. *15*, 243–257.

HOLTON, J. R. (1982), *The role of gravity wave induced drag and diffusion in the momentum budget of the mesosphere*, J. Atmos. Sci. *39*, 791–799.

KATO, S., OGAWA, T., TSUDA, T., SATO, T., KIMURA, I., and FUKAO, S. (1984), *The middle and upper atmosphere radar: First results using a partial system*, Radio Sci. *19*, 1475–1484.

KLOSTERMEYER, J., and RÜSTER, R. (1984), *VHF radar observation of wave instability and turbulence in the mesosphere*, Adv. Space. Res. *4*, 79–82.

LINDZEN, R. S. (1981), *Turbulence and stress owing to gravity wave and tidal breakdown*, J. Geophys. Res. *86*, 9707–9714.

RÖTTGER, J., and IERKIC, H. M. (1985), *Postset beam steering and interferometer applications of VHF radars to study winds, waves, and turbulence in the lower and middle atmosphere*, Radio Sci. *20*, 1461–1480.

RÜSTER, R., and KLOSTERMEYER, J. (1987), *Propagation of turbulence structures detected by VHF radar*, J. Atmos. Terr. Phys. *49*, 743–750.

SATO, T., and WOODMAN, R. F. (1982), *Fine altitude resolution observations of stratospheric turbulent layers by the Arecibo 430 MHz radar*, J. Atmos. Sci. *39*, 2546–2552.

VANZANDT, T. E., GREEN, J. L., GAGE, K. S., and CLARK, W. L. (1978), *Vertical profiles of refractivity turbulence structure constant: Comparison of observations by the Sunset Radar with a new theoretical model*, Radio Sci. *13*, 819–829.

VINCENT, R. A., and REID, I. M. (1983), *HF Doppler measurements of mesospheric gravity wave momentum fluxes*, J. Atmos. Sci. *40*, 1321–1333.

WEINSTOCK, J. (1981), *Energy dissipation rates of turbulence in the stable free atmosphere*, J. Atmos. Sci. *38*, 880–883.

YAMAMOTO, M., TSUDA, T., KATO, S., SATO, T., and FUKAO, S. (1987), *A saturated inertia gravity wave in the mesosphere observed by the Middle and Upper atmosphere radar*, J. Geophys. Res. *92*, 11993–11999.

YAMAMOTO, M., TSUDA, T., KATO, S., SATO, T., and FUKAO, S. (1988), *Interpretation of the structure of mesospheric turbulence layers in terms of inertia gravity waves*, Physica Scripta *37*, 645–650.

(Received September 7, 1987, revised/accepted April 12, 1988)